Sound & Vibration 2026, 60(6), 4624.
doi: https://doi.org/10.59400/sv4624

Article

A spectral-band estimation method of ground acoustic impedance for wind turbine sound propagation

Chao Ma[1,2], **Weifeng Yan**[3], **Shuyu Shen**[1], **Wenzhong Shen**[1,4,*], **Chang Xu**[4]

[1] College of Electrical, Energy and Power Engineering, Yangzhou University, Yangzhou 225127, China; 008656@yzu.edu.cn (CM); ssy.223948@sieyuan.com (SS)
[2] Wuxi Smart Auto-Control Engineering Co., Ltd., Wuxi 214112, China
[3] CGC Jiangsu Test & Certification Limited, Yancheng 224100, China; yanwf@cgc.org.cn
[4] College of Renewable Energy, Hohai University, Changzhou 213200, China; zhuifengxu@hhu.edu.cn
* **Corresponding author:** Wenzhong Shen, wzsh@yzu.edu.cn

CITATION

Ma C, Yan W, Shen S, et al. A spectral-band estimation method of ground acoustic impedance for wind turbine sound propagation. Sound & Vibration. 2026; 60(6): 4624. https://doi.org/10.59400/sv4624

ARTICLE INFO

Received: 5 July 2026
Revised: 28 July 2026
Accepted: 20 August 2026
Available online: 26 August 2026

Abstract: Accurate characterization of ground acoustic impedance is essential for reliable prediction of wind turbine sound propagation over natural and agricultural surfaces. In conventional indirect measurements, a loudspeaker and two microphones at different heights are used to estimate an equivalent flow resistivity by fitting the measured sound pressure level (SPL) differences with those calculated from an image-source propagation model and an acoustic impedance model. Because this fitting is generally carried out over a broad frequency range, the conventional approach is referred to here as the global-band method. However, a single full-band flow resistivity may not represent the frequency-dependent ground response with sufficient accuracy. To improve the spectral representation of the ground boundary condition, this paper proposes a spectral-band method for determining the ground impedance in individual 1/3-octave frequency bands. The method is intended to provide more accurate impedance inputs for wind turbine sound propagation models. The results show that the spectral-band method more accurately captures the frequency-dependent behavior of the effective flow resistivity and ground impedance, significantly reducing the discrepancy between calculated and measured SPL differences. In addition, an empirical formula is established to describe the relationship between the flow resistivity obtained using the global-band method and that obtained using the spectral-band method, so that the ground impedance can be more conveniently specified for simulations at individual frequency bands.

Keywords: wind turbine sound propagation; ground acoustic impedance; acoustic measurement; spectral-band method; flow resistivity

1. Introduction

With the growing global demand for renewable energy, wind power has experienced rapid development worldwide due to its clean and efficient nature [1]. In recent years, the rated power of onshore wind turbines has continued to increase, which may lead to a corresponding rise in wind turbine noise levels in regions near wind farms. This has drawn widespread attention to the issue of noise pollution from wind turbines. The propagation of wind turbine sound to nearby residential areas is influenced by multiple factors, such as air absorption, wind speed, wind direction, distance, ground topography, and temperature [2]. In addition, different types of ground surfaces exhibit distinct acoustic properties that also affect sound propagation [3]. This effect is commonly characterized by the normalized ground acoustic impedance. Therefore, accurately calculating and measuring ground acoustic impedance is essential for improving the precision of sound propagation modeling in wind farms and for reliably assessing their impact on surrounding communities [4].

The relevance of ground impedance to wind turbine applications should be clarified. The present work does not attempt to model the aerodynamic sound generation of wind turbines. Instead, it focuses on the ground boundary condition required by wind turbine sound propagation models. Wind turbines differ from many near-ground environmental sources because the acoustic source is elevated, the receiver is often close to the ground, and long propagation paths lead to a strong interaction between the direct and the ground-reflected sound. In low- and mid-frequency bands, where the atmospheric air absorption is relatively weak, an inaccurate ground impedance may lead to an inaccurate prediction of the ground effect.

To measure the ground acoustic impedance, there exist numerous methods, which are commonly categorized as direct or indirect methods. Direct methods refer to techniques that determine ground acoustic impedance without relying on propagation or impedance models. These methods are typically restricted to laboratory environments due to the complexity and limitations of the equipment and procedures involved, which are often impractical for field use. Although these direct methods are relatively straightforward and effective, they often fall short in accurately characterizing the ground impedance in wind farm environments [5]. Indirect methods, by contrast, rely on sound propagation models and acoustic impedance models. ANSI S1.18 [6] proposes comparing the magnitude of a transfer function with precomputed level difference spectra to determine surface impedance through spectral matching. The image source method [7] combined with the Delany–Bazley single-parameter ground impedance model [8] has been used to fit the flow resistivity parameter, enabling the estimation of ground impedance. This method is particularly suitable for determining the best-fit/effective flow resistivity that best fits the measured data within a small spatial measurement area, making it experimentally convenient. However, due to the short microphone spacing involved, the lower limit of the applicable frequency range is about 500 Hz. Martens et al. [9] applied the inclined path method to classify the ground impedance across different surface types, including forest soil, grassland, and bare sandy ground. Bérengier et al. [10] investigated the acoustic properties of porous road surfaces using a combination of the image source method and a porous ground model. These approaches are all considered indirect methods. The Nordtest method [11] is a typical example of an indirect approach used to determine the flow resistivity class of flat outdoor ground surfaces by matching measured data over a target frequency range with precomputed results. Based on a specified geometry, ground impedance can then be derived from the fitted flow resistivity. Due to constraints in geometry and the use of the Delany–Bazley [8] model, the method is valid within a frequency range of 200–2,500 Hz. Recently, Nyborg and Shen [12] introduced a novel measurement technique designed for wind farm applications. By developing a new geometric configuration, their method successfully extends the lower bound of the applicable frequency range down to 50 Hz, but the sound incidence angle is the same as the Nordtest method [11]. Guillaume et al. [13] proposed a two-microphone method with a semi-automated inversion routine, which estimates ground impedance parameters by fitting the measured sound-pressure-level attenuation spectrum to the analytical solution for the specified source–receiver configuration. Liu et al. [14] proposed a multi-geometry method to ensure the uniqueness of parameter determination in acoustic impedance models for green roofs, and demonstrated its effectiveness on typical porous materials. Cobb et al. [15] reported the results obtained when applying the ANSI/ASA S1.18 standard [6] for outdoor acoustic surface impedance measurement to surfaces whose characteristics fall within or beyond the recommended use cases.

Different attenuation models employ varying approaches to calculate ground effects. In engineering calculations based on ISO 9613-2 [16], the ground effect is commonly simplified through ground factors selected according to the ground type, for instance, hard or porous ground. Such simplification is useful for practical assessments, but it does not explicitly provide the complex impedance required by wave-based models such as the parabolic equation (PE) method. For wind turbine applications, this distinction is important because the source is elevated, the receiver height may be close to the ground during acoustic measurements, and the propagation distance is much larger than the local impedance-measurement geometry. According to IEC 61400-11 [17], the microphone height used in wind turbine noise measurements is close to the ground, for example at 1.7 m height, whereas the effective source height of a wind turbine is related to the hub height and blade positions. Therefore, a local acoustic-impedance measurement should not be interpreted as a scaled reproduction of a whole wind turbine. It should instead be considered a method for estimating a ground boundary parameter that can subsequently be used in wind turbine sound propagation simulations.

To improve the accuracy of ground acoustic impedance estimation using indirect methods, a variety of acoustic impedance models have been developed. Among these, the Delany–Bazley model [8] is the most widely used single-parameter ground impedance model, in which flow resistivity is the sole parameter. Building on this, Miki [18] proposed a modified version that retains the single-parameter structure, still using flow resistivity as the only input. However, single-parameter models may not adequately represent the complex physical characteristics of natural soils. Moreover, single-parameter models are physically inadmissible. Even with modifications to ensure surface-impedance passivity, they still violate the physical constraint that the real part of the complex density be positive [19]. As a result, multi-parameter impedance models have been introduced. Attenborough [20] developed a two-parameter model by incorporating the porosity variation rate alongside flow resistivity. This model assumes that porosity varies exponentially with depth, aligning well with the nature of real soil and yielding more accurate results, particularly at low frequencies and for highly resistive grounds. He later proposed a four-parameter model [21], which includes porosity, grain shape factor, shape factor of pores, and flow resistivity, providing a physically meaningful and precise representation of soil acoustic properties. For further information on various ground impedance models, readers may refer to ANSI S1.18 and the study of Attenborough et al. [22,23]. Since the porosity is typically unknown in practice, it must be obtained through in-situ measurements, increasing the complexity of experiments. To address this, Raspet and Sabatier [24] and Salomons incorporated the porosity-depth variation into an equivalent complex medium governed by the Euler and continuity equations. The solutions to the resulting wave equation provide physically meaningful results regarding porosity. Attenborough [25–27] also proposed porosity-based models and corrections. However, these models often require the introduction of additional parameters, making them more computationally intensive. As a result, typical parameter values are often used instead. Nonetheless, the variation in soil characteristics across different ground types can lead to significant modeling errors when using default values. To overcome this issue, Wu et al. [28] introduced a parameter optimization approach using the MATLAB fmincon function to identify optimal model parameters. Fuchs and Haider [29] calculated the effective flow resistivity of the ground surface via least-squares optimization and examined the applicability of various impedance models. Ghiasvand et al. [30] combined physically guided pseudo-well augmentation with a feedforward neural network, providing a practical and computationally efficient approach for acoustic impedance inversion in data-limited offshore environments. Machine learning has been widely applied to acoustic boundary layer inversion [31] and acoustic surface impedance inversion [32].

In addition to the above modeling efforts, several studies have further investigated the influence of ground and surface impedance on sound propagation under specific environmental conditions. Vecchiotti et al. [33] demonstrated through numerical simulations over rough sea surfaces that the use of an equivalent surface impedance has inherent limitations. Attenborough [34] developed an approximate analytical model for A-weighted broadband sound propagation over flat soft ground, incorporating frequency-independent parameters to account for ground effect, turbulence, and refraction, which showed better agreement with measurements for onshore wind turbine noise than standard simplified methods. Vecchiotti et al. [35] achieved a better agreement (<2 dB) by accounting for absorption inhomogeneity through direct measurements of effective flow resistivity.

Considerable efforts have been devoted to studying the influence of acoustic impedance on sound propagation within the framework of propagation modeling. Cao et al. [36] and Delany and Bazley proposed a novel high-fidelity sound propagation model. In this model, the four-parameter acoustic impedance model proposed by Attenborough [21] is employed. Colas et al. [37] proposed a new approach to wind turbine noise propagation employing the linearized Euler equations, with the ground surface impedance characterized by a variable-porosity model [20]. Nyborg et al. [38] systematically examined the impact of varying flow resistivity on acoustic impedance using different formulations of the PE method. Naylor and Qin [39] simulated the sound propagation over rough ground by incorporating a modified effective impedance model into a parabolic equation code. Horsman et al. [40] investigated sea-surface-related ground effects for offshore wind turbine noise propagation by comparing the effective flow resistivity under three water surface conditions using an approach similar to the two-microphone method. Nguyen et al. [41] predicted noise levels at multiple receiver locations using a numerical ray-tracing propagation model in conjunction with nine ground impedance models, and observed that the variability among these impedance models represents a notable source of uncertainty.

However, it is worth noting that the Nordtest method [11] estimates the ground impedance based on the entire frequency band of interest (typically 200–2,500 Hz). In the above references, the acoustic impedance used was computed over the full frequency range without considering individual octave or one-third octave bands. The observed variation of impedance with flow resistivity primarily resulted from the frequency dependence inherent in the impedance model, rather than reflecting any intrinsic frequency dependence of the flow resistivity itself.

In response to this limitation, the present study proposes a frequency-band-specific approach that estimates the ground impedance for one-octave or one-third-octave frequency bands individually. To avoid ambiguity, this approach is referred to in this paper as the spectral-band method, in contrast to the traditional global-band method.

This paper is organized as follows. Section 1 provides an overview of the development of ground acoustic impedance models. Section 2 describes the experimental setup and ground surface conditions. Section 3 details the calculation methodology, and the results are presented in Section 4. Finally, Section 5 summarizes the main conclusions of this study.

2. Measurement set-up

This study analyzed experimental data from four sets of experiments. These four experiments (Tests 1–4) all employed the same geometric configuration but were conducted under different surface conditions, with the aim of verifying the general applicability of the proposed method across various ground types.

The measurement geometry shown in **Table 1** is not intended to directly simulate the source-receiver geometry of a full-scale wind turbine. Instead, a speaker-microphone array was used to characterize the local in-situ soil resistance under controlled outdoor conditions. The impedance obtained is intended to serve as the ground boundary condition for subsequent calculations of sound field propagation from wind turbines. However, the actual height of the wind turbine sound source, the height of the receiving point, the terrain, and meteorological conditions must be specified separately.

Table 1. Summary of ground surface conditions, measurement geometries, and equipment specifications (microphones and sound sources) for four test cases.

Parameters	Test 1	Test 2	Test 3	Test 4
Height of source [m]	0.5	0.5	0.5	0.5
Height of top microphone [m]	0.5	0.5	0.5	0.5
Height of bottom microphone [m]	0.2	0.2	0.2	0.2
Distance between source and microphone [m]	1.75	1.75	1.75	1.75
Ground type	Harvested dry grassland	Dry short grass lawn	Soft farmland after stalk harvesting	Flattened farmland
Location	RISO	Yizheng	Yizheng	Hanjiang
Microphone brand	Norsonic Nor1218	GRAS 46AZ	GRAS 46AZ	GRAS 46AZ
Source brand	Brüel & Kjær 4595	AWA 5512	AWA 5512	Genelec 8361A

To provide a clearer overview of the four experimental setups, **Table 1** summarizes the key information for reference.

The microphones and loudspeakers used in this study comply with the requirements of the Nordtest method [11]. Specifically, the method requires a source with a directivity variation within 1 dB over ±45°, and microphones with a directivity variation within 1 dB over ±30°. All microphones were fitted with windshields. Additional experimental conditions, including surface flatness, measurement procedures, and environmental parameters, conformed to the Nordtest specifications. For further methodological details, readers are encouraged to consult [11].

3. Methodology

In this section, the following methods are summarized: the sound pressure level calculation formula proposed by Nyborg and Shen [12] using the image source method, the Attenborough four-parameter (4P) ground acoustic impedance model [23], and the optimization method for determining the impedance-model parameters proposed by Wu et al. [28]. To determine ground acoustic impedance more accurately, the present study develops a spectral-band method in which the inversion is carried out separately in each frequency band. This procedure also increases the resolution of the candidate flow-resistivity levels within a physically reasonable range.

3.1. Sound pressure level calculation formula

The image source method is presented in **Figure 1**, where the propagation of a sound wave from a source at height H_s to a receiver at height H_r with a separation distance of d is considered.

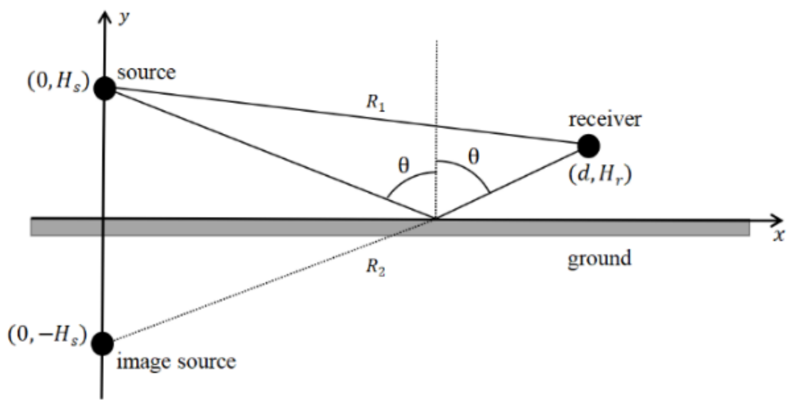

Figure 1. Illustration of the image source method: a source and a receiver are positioned above the ground, with a mirrored (image) source located symmetrically beneath the ground surface [28].

More details regarding the geometric configuration can be found in the work of Fauri [42]. Based on this method, Nyborg and Shen [12] proposed the following formula for calculating the SPL:

$$L_p = S + 10\log\left(1 + \frac{R_2^2}{R_1^2}|Q|^2 + \frac{2R_1|Q|}{R_2}\cos\left(k\left(R_2 - R_1\right) + \varphi\right)\right) - 10\log\left(4\pi R_1^2\right) \qquad (1)$$

where, S is the sound source amplitude level, R_1 is the direct path length between the source and the receiver, R_2 is the path from the image source to the receiver, k is the acoustic wavenumber, Q is the spherical wave reflection coefficient, and φ denotes the phase angle of Q. The spherical wave reflection coefficient is expressed as follows:

$$Q == \frac{\cos(\theta) - Z^{-1}}{\cos(\theta) + Z^{-1}} E(\rho) \tag{2}$$

where, θ is the angle of reflection, Z is the normalized ground acoustic impedance.

3.2. Impedance model

To investigate the impedance characteristics of porous materials, Attenborough proposed a four-parameter model [21]. This model is capable of delivering results with higher precision and is adopted in this study. The model is expressed by the following formulas:

$$k_g = \frac{\omega}{c}\sqrt{\gamma\Omega}\sqrt{\left(\frac{4}{3} - \frac{\gamma - 1}{\gamma}N_{pr}\right)\frac{q^2}{\Omega} + i\frac{s_f^2\sigma}{\rho\omega}} \tag{3}$$

$$Z = \left(\frac{4q^2}{3\Omega} + i\frac{s_f^2\sigma}{\rho\omega}\right)\frac{\omega}{c}\frac{1}{k_g} \tag{4}$$

where, $\omega = 2\pi f$ is the angular frequency, the speed of sound is taken as c = 340 m/s, the specific heat ratio of air is γ = 1.4, the Prandtl number is approximately $N_{pr} \approx 0.7$, and the air density is $\rho = 1.2$ kg/m^3, and $q^2 = \Omega^{-g}$ represents the tortuosity squared. Here, Ω is the porosity, g is the grain shape factor, s_f is the pore shape factor, and σ is the flow resistivity. These four parameters must be determined based on the actual ground conditions. This paper first adopts the method proposed by Wu et al. [28] to compute the optimal parameters, which are then listed in **Table 2**.

Table 2. Optimal values of the four parameters for the four grounds.

Test campaigns	Ω [-]	g [-]	s_f [-]
Test 1	0.5417	0.7172	0.7959
Test 2	0.5428	0.3448	0.8186
Test 3	0.5225	0.4248	0.8838
Test 4	0.5372	0.3150	0.8327

3.3. Spectral-band calculation method of ground acoustic impedance

The Nordtest method [11] provides an indirect approach to estimating the ground acoustic impedance by minimizing the discrepancy between computed and measured SPL differences obtained with two vertically aligned microphones over the frequency range of 200–2,500 Hz. However, because the minimization is performed over the whole target frequency range, it does not explicitly provide a separate impedance estimate for each 1/3-octave band. To address this limitation, the present study proposes a spectral-band method that estimates the ground impedance independently in each 1/3-octave band. In this paper, the term "best-fit flow resistivity" denotes the effective flow resistivity that minimizes the discrepancy between the measured and calculated SPL differences within a specified frequency band. It should not be interpreted as a directly measured intrinsic soil property, but as an equivalent acoustic parameter within the adopted impedance and propagation models.

While the overall computational framework of the proposed method is consistent with the Nordtest approach [11], it differs in that the error minimization is performed separately for each 1/3-octave frequency band rather than over the entire frequency range. The band-wise fitting error is defined as $e_f = |\Delta L_{\text{meas},f} - \Delta L_{\text{cal},f}|$, where ΔL is the SPL difference between the upper and lower microphones. The total fitting error is defined as $E_{\text{sum}} = \sum_{f\in F} e_f$ over the considered bands. These definitions are used only as fitting metrics; lower values indicate better agreement between the calculation and the measurement. The procedure consists of the following steps.

1. Calculate the difference in sound pressure level (SPL) between the upper and lower microphones based on multiple measurements, and compute the mean and standard deviation to evaluate the validity of the experimental data.
2. Through parameter optimization, obtain the best-fit or effective parameters that characterize the foundation properties.
3. Based on the optimized parameters, the underground flow resistance can be calculated. The calculated sound pressure level difference is closely related to the selected flow resistance value. The Nordtest method [11] provides 12 discrete flow resistance levels; however, since the sites measured in this study are all natural ground or similar terrain (such as muddy ground or farmland), previous research and practical experience indicate that reasonable flow resistance values typically range from 10 to 1,000 kN·s/m^4. It should be noted, however, that the intervals between flow resistance levels in the Nordtest method are relatively large. This may result in poor agreement between the measured sound pressure level differences and the calculated results, thereby introducing significant uncertainty in the final determination of the best-fit or effective flow resistance value. To improve the agreement between theoretical calculation results and measured data, this study employs a finer grid with smaller increments to refine the flow resistance values within the 10–1,000 kN·s/m^4 range. This approach more accurately reflects the actual acoustic properties of the subsurface. To avoid unnecessary computational costs associated with using overly fine flow resistance grids throughout the entire calculation process, this study adopts a two-stage calculation scheme. Initially, a coarse set of flow resistivity is used: 10, 16, 25, 40, 63, 100, and 150 kN·s/m^4, followed by increments of 50 kN·s/m^4 up to 1,000 kN·s/m^4. The first six values are based on the Nordtest method [11], which has a relatively narrow range. The subsequent settings with larger increments are intended to balance computational efficiency and fitting accuracy.
4. From the results of these selected flow resistivities, a smaller interval range can be identified in which calculated and measured SPL differences closely match. Within this range, the calculated SPL difference is calculated with a step size of 1 kN·s/m^4. Finally, the flow resistivity corresponding to the minimum error between calculated and measured SPL differences is determined for each 1/3 octave frequency band.
5. Calculate the real and imaginary parts of the acoustic impedance for each one-third

octave band based on the final flow resistivity values obtained for each frequency band.

Although 1/3-octave bands were selected in this study due to their common usage in noise analysis, the proposed method is generalizable and can be applied to other frequency resolutions, such as 1/1- or 1/12-octave bands, etc.

4. Results and discussion

To evaluate the differences and accuracy between the spectral-band method and the global-band method, the measurement results from four experimental campaigns, as described in Section 2, are analyzed and discussed below.

4.1. Comparison of the new and original methods based on different ground types

In this subsection, the performance of the newly proposed spectral-band method is evaluated against the traditional global-band method by analyzing experimental data obtained under identical geometric conditions but on four different ground surfaces, as introduced in Section 2. This comparison aims to investigate how each method handles variations in ground surface properties and to assess the accuracy and reliability of the impedance estimations.

4.1.1. Accuracy assessment of the methods

The performance of the spectral-band method was further examined for the four ground types introduced in Section 2. The purpose was to determine whether the method remains applicable when the acoustic properties of the ground change. The following figures present the best-fit impedance results obtained from both the spectral-band and global-band approaches under different test conditions and excitation signals. For each case, the calculated SPL differences were compared with the corresponding measurements. The level of agreement varies across frequency ranges and ground surfaces, allowing the fitting accuracy and limitations of the two approaches to be assessed more directly. These comparisons also provide the basis for the subsequent discussion of the acoustic characteristics of the tested ground surfaces.

Figure 2 shows the fitting results for Test 1, in which white noise was used as the excitation signal. In the frequency ranges of 200–800 Hz and 1,250–2,500 Hz, the SPL differences predicted by the spectral-band method generally follow the measured values more closely, and the corresponding fitting errors remain relatively small. A noticeable exception occurs near 1,000 Hz, where the discrepancy becomes much larger. The reason for this local increase is not immediately clear and may be related to the frequency-dependent response of the ground or to uncertainties in the measurement. The global-band method gives a less satisfactory fit overall. Since the same flow resistivity is applied to the entire frequency range, the resulting impedance model cannot fully represent changes in ground behavior from one band to another. This limitation becomes more apparent in frequency regions where the measured SPL difference changes rapidly.

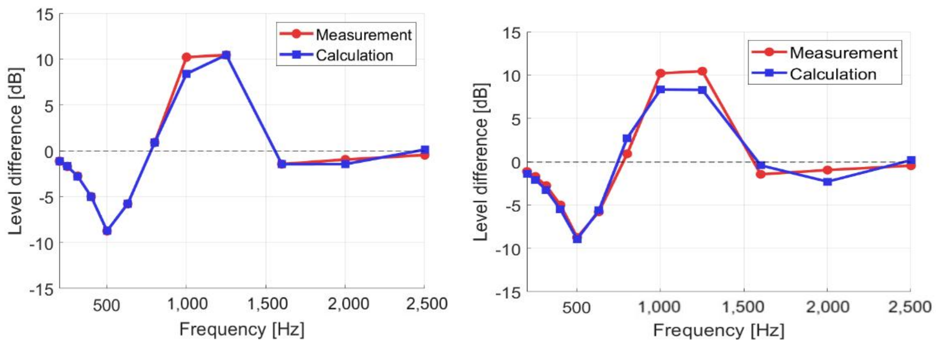

(a) **(b)**

Figure 2. SPL difference obtained from the measurements and from the calculation in Test 1 using white noise: **(a)** spectral-band method; **(b)** traditional global-band method.

A similar pattern can be seen in **Figure 3** for Test 2. Although the difference between the two methods is small in several bands, the spectral-band approach agrees more closely with the measurements over most of the frequency range. **Figures 4** and **5** present the corresponding results for Tests 3 and Test 4. The degree of improvement varies among the tests, but the spectral-band method produces the lower fitting error in most cases. Taken together, these results support the earlier observation that treating the impedance parameters on a band-by-band basis provides a more accurate description of the measured ground effect than using one parameter value for the full spectrum.

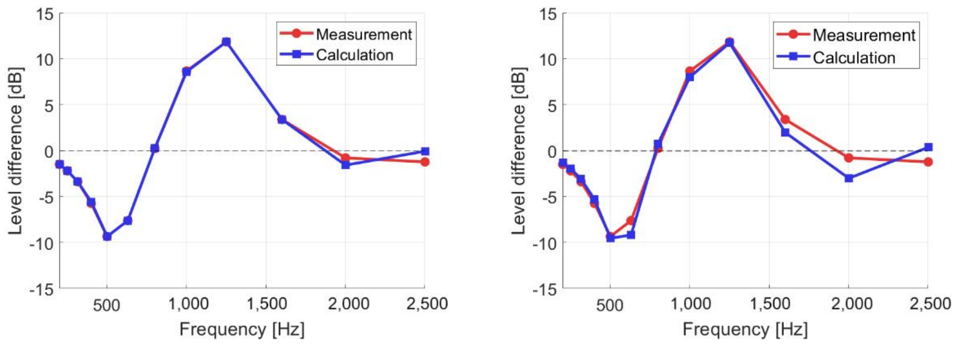

(a) **(b)**

Figure 3. SPL difference obtained from the measurements and from the calculation in Test 2 using white noise: **(a)** spectral-band method; **(b)** traditional global-band method.

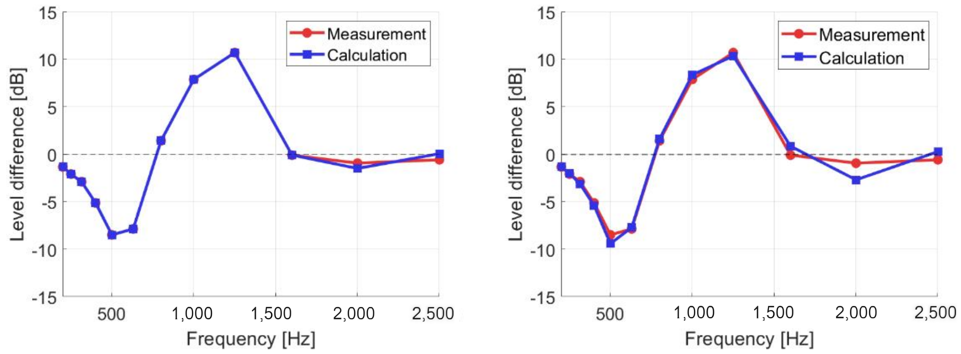

(a) **(b)**

Figure 4. SPL difference obtained from the measurements and from the calculation in Test 3 using white noise: **(a)** spectral-band method; **(b)** traditional global-band method.

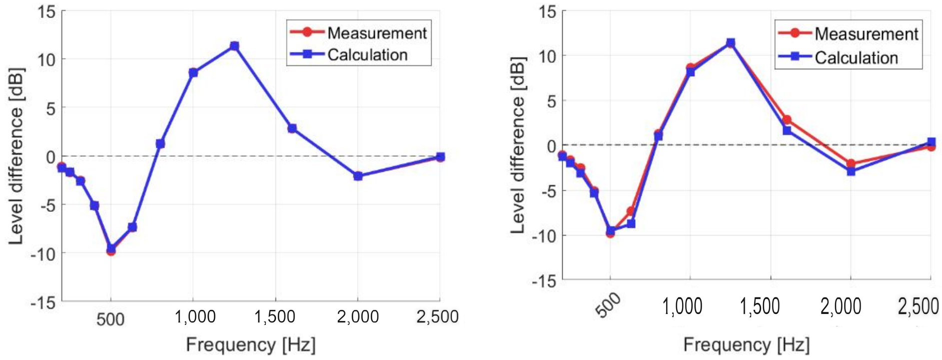

(a) **(b)**

Figure 5. SPL difference obtained from the measurements and from the calculation in Test 4 using white noise: **(a)** spectral-band method; **(b)** traditional global-band method.

The improved performance of the spectral band method highlights the importance of accounting for the frequency dependence of ground impedance. Different types of ground surfaces exhibit varying acoustic behavior across frequency bands due to variations in soil structure, moisture content, and other physical properties. By estimating the impedance for each frequency band separately, this method can capture these variations more accurately. This is particularly critical for natural or agricultural sites. If a single global parameter is assumed, the model becomes overly simplified, thereby reducing the reliability of the predictions.

To more clearly demonstrate the accuracy, **Figure 6** uses bar charts to compare the band-wise fitting errors between the measured and calculated SPL differences for each 1/3-octave-band center frequency. The term "fitting error" refers to the absolute difference between the measured and calculated SPL differences in a specific band, and the "total fitting error" is the sum of these absolute errors over all considered bands.

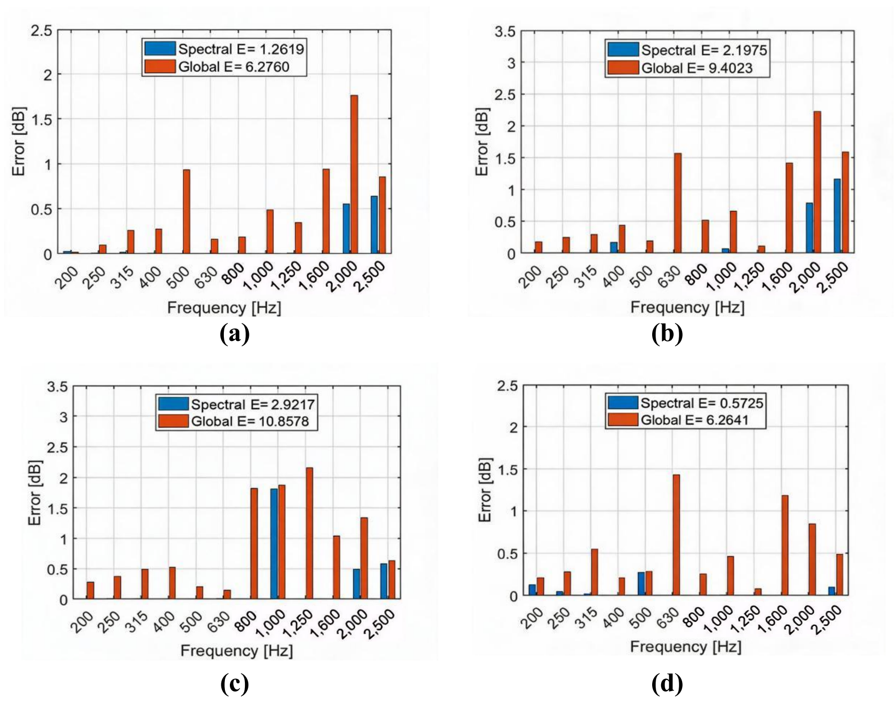

Figure 6. Comparison of SPL discrepancies between measured and calculated results using the spectral-band and traditional global-band methods: **(a)** Test 1; **(b)** Test 2; **(c)** Test 3; **(d)** Test 4.

Figure 6a presents the fitting-error results in Test 1 using white noise as the excitation signal. The total fitting error for the global-band method is 10.9 dB, whereas the spectral-band method reduces this value to 2.9 dB. Except for the 1,000 Hz band, where an increased fitting error is observed, errors in the other bands are notably reduced. The relatively larger deviation around 1,000 Hz in Test 1 may be associated with local ground inhomogeneity, reduced signal-to-noise ratio, or a transition region in which a single equivalent flow resistivity is less representative of the actual ground response. Since this deviation is not observed consistently in Tests 2–4, it is not considered a systematic limitation of the spectral-band method.

Figure 6b–d correspond to the results in Tests 2–4, respectively, under white noise excitation. The total errors for the global frequency band method are 9.4 dB, 6.3 dB, and 6.3 dB, whereas the per-frequency-band method reduces the errors to 2.2 dB, 1.3 dB, and 0.6 dB, respectively. Across all the bands, the spectral-band method achieves an improved fit performance, and no significant spikes in error were observed in any frequency band. In summary, the spectral-band method consistently delivers lower fit errors under all test conditions, demonstrating superior accuracy. This makes it particularly suitable for scenarios where the ground acoustic impedance exhibits a strong frequency dependence.

4.1.2. Comparison of impedance estimation results

To assess the applicability of the spectral-band method under varying ground types, **Figure 7** shows the impedance variation trends in Tests 1–4 under white noise excitation, further demonstrating the applicability of the spectral-band method across different ground types.

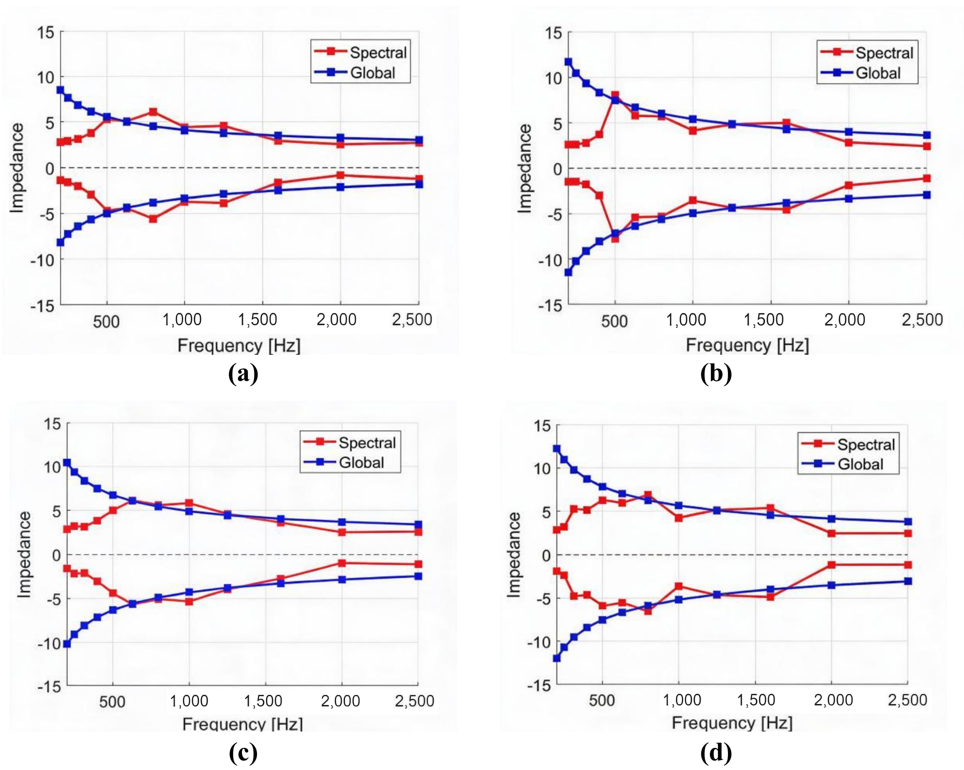

Figure 7. Real (upper) and imaginary (lower) components of the estimated complex ground impedance using the spectral-band method and the traditional global-band method: **(a)** Test 1; **(b)** Test 2; **(c)** Test 3; **(d)** Test 4.

As shown in **Figure 7a**, on dry and freshly mown grassland, both the real and imaginary parts of the acoustic impedance obtained using the spectral-band method increase with frequency up to 800 Hz, and then decrease as the frequency continues to rise. This trend differs from that obtained by the global-band method, which shows a monotonic decrease in impedance with increasing frequency.

In **Figure 7b**, for dry lawn surfaces, the real and imaginary parts of the impedance derived from the spectral-band method increase with frequency up to 800 Hz, then decrease between 800 and 1,000 Hz. Beyond this range, they exhibit a fluctuating pattern of increase followed by decrease. Overall, both components reach their maximum values around 800 Hz. In contrast, the global-band method still produces impedance values that continuously decrease with frequency.

Figure 7c illustrates that for freshly harvested farmland, the real and imaginary components of impedance obtained via the spectral-band method increase with frequency below 630 Hz. Between 630 and 1,000 Hz, the impedance first decreases and then increases, followed by a general decline at higher frequencies.

In **Figure 7d**, for compacted and leveled farmland, the impedance components increase with frequency below 500 Hz, show a decreasing trend between 500 and 1,000 Hz, rise again between 1,000 and 1,600 Hz, and then decrease beyond 1,600 Hz.

The results show that the spectral-band method more sensitively captures the frequency-dependent interaction between the acoustic field and the ground surface across multiple bands. It is particularly effective in revealing the non-stationary behavior in ground impedance over specific frequency ranges. In contrast, the global-band method applies a single set of parameters across all frequencies. While this yields smoother and more continuous results, it often obscures important features in certain bands, leading to a reduced resolution in impedance modeling.

In summary, although the spectral-band method may be somewhat less continuous across the entire frequency range, it offers clear advantages in resolving frequency-specific features, improving the local fit precision, and capturing the complex acoustic behavior of ground surfaces. It is therefore especially suitable for acoustical research and engineering applications that are sensitive to frequency-domain characteristics.

To investigate the relationship between the flow resistivity obtained using the spectral-band method and that obtained using the global-band method, a comparative analysis was conducted based on the results of the four test cases, as shown in **Figure 8**.

Figure 8a illustrates the relationship and variation trends of flow resistivity determined by the spectral-band method and by the global-band method in Test 1. It can be observed that the flow resistivity determined by the spectral-band method shows an overall increasing trend. In the 800–1,600 Hz range, the values fluctuate around those determined by the global method, while in the higher frequency range (2,000–2,500 Hz), the resistivity gradually decreases and remains below the value obtained from the global fit method.

Figure 8b,c, corresponding to Test 2 and Test 3, exhibit trends similar to those observed in Test 1. In the low-frequency range (200–630 Hz), flow resistivity increases with frequency. In the mid-frequency range (800–1,600 Hz), although the resistivity varies more complexly, it still fluctuates slightly around the global value. In the high-frequency range (2,000–2,500 Hz), the values obtained by the spectral-band method are consistently lower than those from the global method.

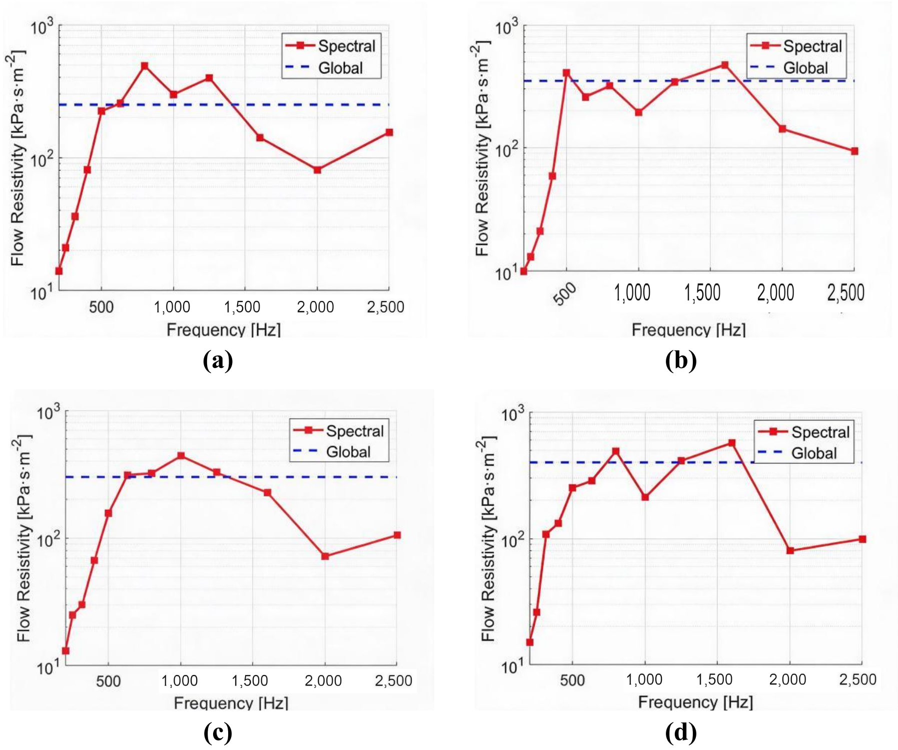

Figure 8. Relationship between the flow resistivities determined by the spectral-band method and by the traditional global-band method: **(a)** Test 1, **(b)** Test 2, **(c)** Test 3, **(d)** Test 4.

Figure 8d presents the relationship between the flow resistivities obtained using both methods in Test 4. In this case, the flow resistivity increases with frequency in the 200–500 Hz range, fluctuates around the global method values between 630–1,600 Hz, and shows a declining trend in the high-frequency range, remaining lower than the values given by the global-band method.

From the results shown in **Figure 8**, it is evident that in the low-frequency range (200–630 Hz), the effective flow resistivity obtained by the spectral-band method increases with frequency, demonstrating a clear spectral dependence. In the mid-frequency range (800–1,600 Hz), the variation is more pronounced, but the values generally fluctuate around the global-band estimate. In the high-frequency range (2000–2,500 Hz), the spectral-band method consistently yields lower effective flow resistivity than the global-band method. Therefore, the global-band estimate can be regarded as a reasonable approximation mainly in the mid-frequency range, whereas it tends to overpredict the effective flow resistivity in both low- and high-frequency bands. This behavior indicates that the spectral-band method is more sensitive to the acoustic response of ground materials across frequencies and provides more physically meaningful inputs for ground modeling and parameter inversion.

4.1.3. Empirical fit of flow resistivity estimates

Due to the complexity of acoustic impedance measurements, determining the impedance by the spectral-band method can be relatively cumbersome. To facilitate the acquisition of flow resistivity and acoustic impedance for each frequency band, an empirical relationship was established. This allows the flow resistivities for individual bands to be estimated from the full-band flow resistivity, which can be obtained either through measurement or literature. The empirical formula is expressed as follows:

$$\sigma(f) = \sigma_{\text{global}} \cdot \left[1 - 0.96 \cdot \exp\left(-\frac{(f-250)^2}{2 \times 180^2}\right)\right] \tag{5}$$

where, σ_{global} denotes the flow resistivity obtained over the full frequency band, while f represents the frequency corresponding to each band.

Figure 9 presents a comparison between the flow resistivities estimated using the proposed empirical formula and the original values obtained from the spectral-band method. As illustrated in the figures, the empirical formula captures the overall frequency-dependent spectral shape of the effective flow resistivity across most 1/3-octave bands. However, a larger discrepancy is observed in one isolated band in each test case, for example around 800 Hz, 1 kHz, or 500 Hz depending on the ground surface. These discrepancies may occur near transition bands where the equivalent flow resistivity changes rapidly with frequency, and where finite-band averaging, local ground inhomogeneity, or measurement uncertainty becomes more influential. The empirical formula is useful when a convenient estimate of impedance is sufficient, but direct spectral-band inversion remains preferable in applications where greater accuracy is needed.

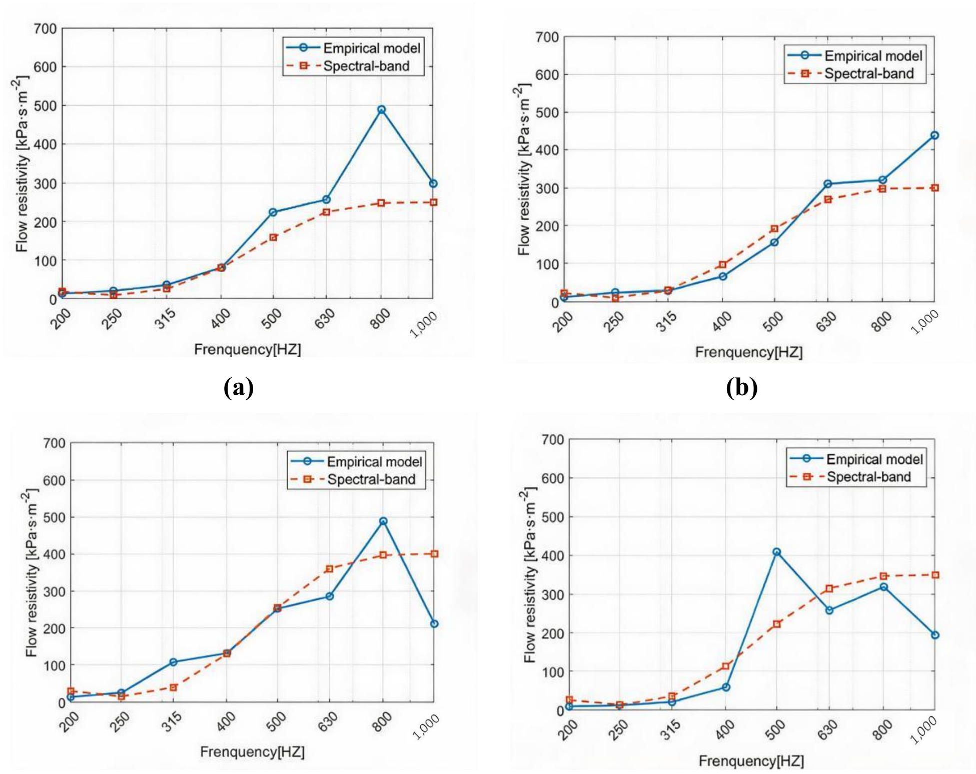

Figure 9. Comparison between the flow resistivities estimated by the empirical formula and those obtained by the spectral-band method: **(a)** Test 1; **(b)** Test 2; **(c)** Test 3; **(d)** Test 4.

Figure 10 compares the real and imaginary components of ground acoustic impedance obtained in two ways. One set of values was calculated using the flow resistivity predicted by the empirical formula, while the other was derived directly from spectral-band inversion for each one-third-octave band.

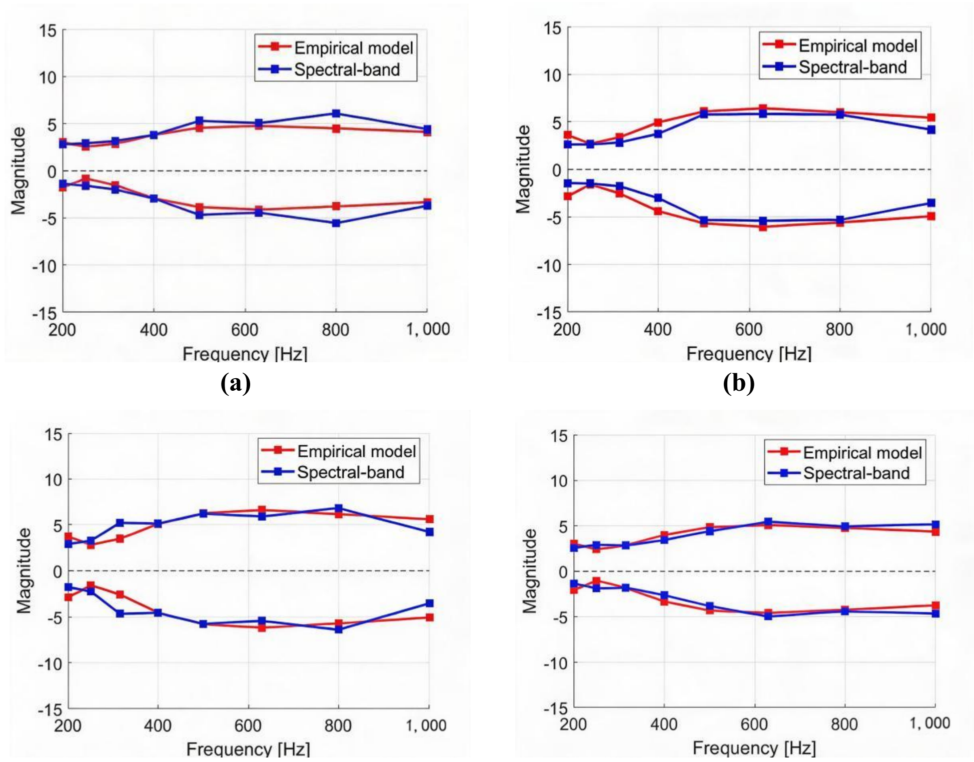

Figure 10. Real (upper) and imaginary (lower) components of the estimated complex ground impedance using the empirical model and the spectral-band method: **(a)** Test 1; **(b)** Test 2; **(c)** Test 3; **(d)** Test 4.

For most frequency bands, the two sets of impedance results are close. This suggests that the empirical relationship can recover the main frequency-dependent features of ground impedance from the full-band flow resistivity. Some differences remain at individual frequencies. These deviations may result from the assumptions introduced in the impedance model, as well as from uncertainty in the measured data. Even so, the overall agreement indicates that the empirical formula provides a reasonable approximation when a simpler impedance estimation procedure is preferred. Direct spectral-band inversion, however, remains more appropriate when detailed band-specific accuracy is required.

4.2. Verification of the spectral-band method using the 1/1-octave band

The spectral-band method was further examined using 1/1-octave bands to determine whether its performance changes as the bandwidth increases. Tests 1–4 were included in the analysis. Attention was given to three aspects: fitting accuracy, estimation of flow resistivity, and the method's response to frequency-dependent acoustic behavior. The results were then compared with those obtained from the 1/3-octave-band analysis. This comparison makes it possible to assess whether the method remains reliable when a broader range of frequency components is represented by a single octave-band value.

4.2.1. Accuracy assessment of the methods

Under the 1/1-octave band condition, the fitting accuracy of the ground acoustic impedance obtained using the conventional full-band method and the newly proposed spectral-band method is illustrated in **Figures 11–14**, corresponding to Tests 1–4.

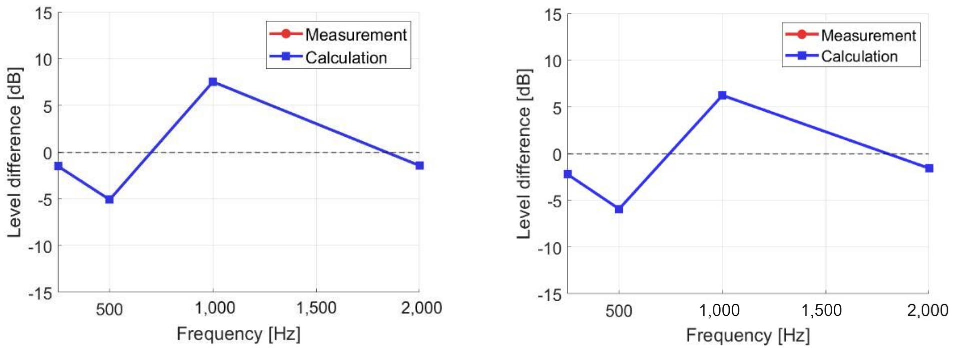

(a) **(b)**

Figure 11. SPL difference obtained from the measurements and from the calculation in Test 1 using white noise based on the 1/1-octave band: **(a)** spectral-band method; **(b)** traditional global-band method.

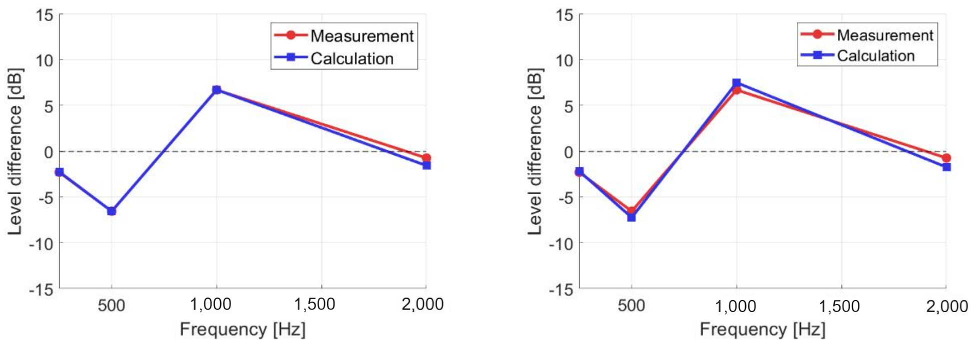

(a) **(b)**

Figure 12. SPL difference obtained from the measurements and from the calculation in Test 2 using white noise based on the 1/1-octave band: **(a)** spectral-band method; **(b)** traditional global-band method.

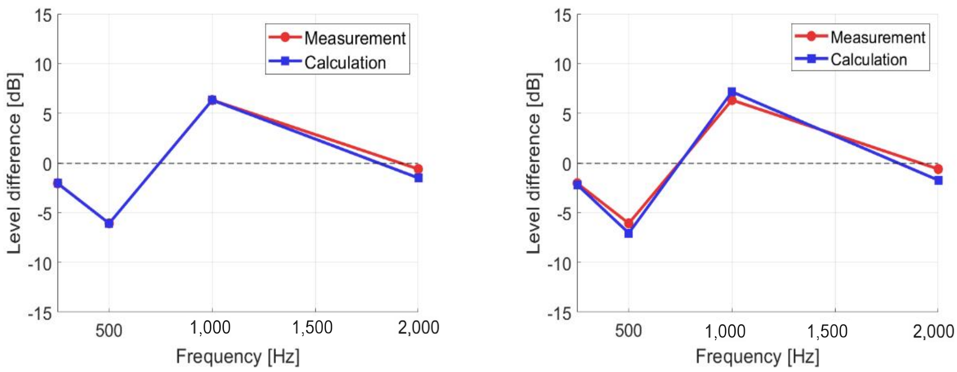

(a) **(b)**

Figure 13. SPL difference obtained from the measurements and from the calculation in Test 3 using white noise based on the 1/1-octave band: **(a)** spectral-band method; **(b)** traditional global-band method.

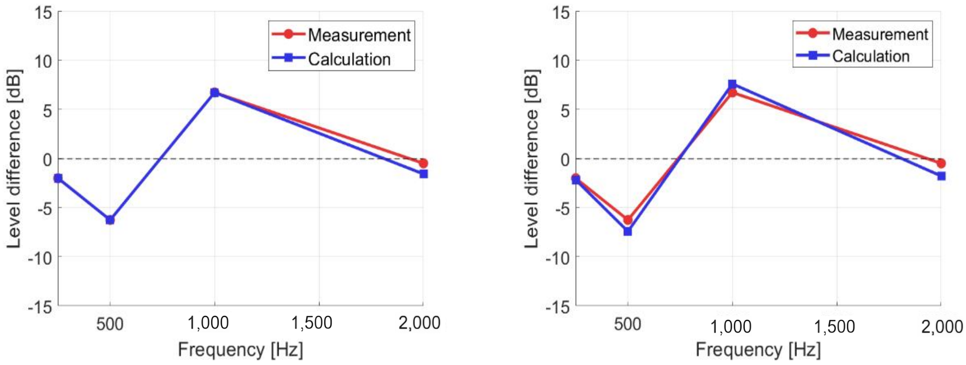

(a) **(b)**

Figure 14. SPL difference obtained from the measurements and from the calculation of Test 4 using white noise based on 1/1-octave band: **(a)** spectral-band method; **(b)** traditional global-band method.

These figures clearly demonstrate that the spectral-band method consistently yields higher fitting accuracy across all surface types and test cases, particularly in capturing the frequency-dependent variations of the impedance. Unlike the global-band method, which tends to smooth out local variations, the spectral-band method reveals more detailed and physically meaningful impedance structures. This superiority is consistently observed across different ground conditions.

The spectral-band method was also tested using 1/1-octave bands. Between 250 and 2,000 Hz, the reconstructed impedance generally agrees well with the measured results, indicating that the method remains reliable within this frequency range. The fit becomes somewhat poorer at 2,500 Hz. One possible reason is the increasing bandwidth of octave bands at higher center frequencies: the 2,500 Hz band contains a relatively broad range of frequency components, whose impedance values may not vary in the same way. Representing the response of the entire band with a single effective impedance is therefore less accurate, particularly when the impedance changes rapidly with frequency. The verification was limited to octave bands at and above 250 Hz. Consequently, no conclusion can yet be drawn about the method's performance below this frequency, even though this range is important in studies of low-frequency wind turbine noise. Further validation at lower frequencies would require either a larger measurement configuration or additional data collected specifically for low-frequency conditions.

These findings are consistent with earlier conclusions drawn under the 1/3-octave band condition and further confirm that the spectral-band method remains both effective and robust, even when extended to wider bandwidths such as the 1/1-octave band. Therefore, it can be regarded as a reliable and generalizable approach for accurate estimation of the ground impedance across a wide range of practical scenarios and frequency resolutions.

4.2.2. Comparison of impedance estimation results

This part presents the ground acoustic impedance calculated using the spectral-band method and the full-band method under the 1/1-octave band condition, as shown in **Figure 15**.

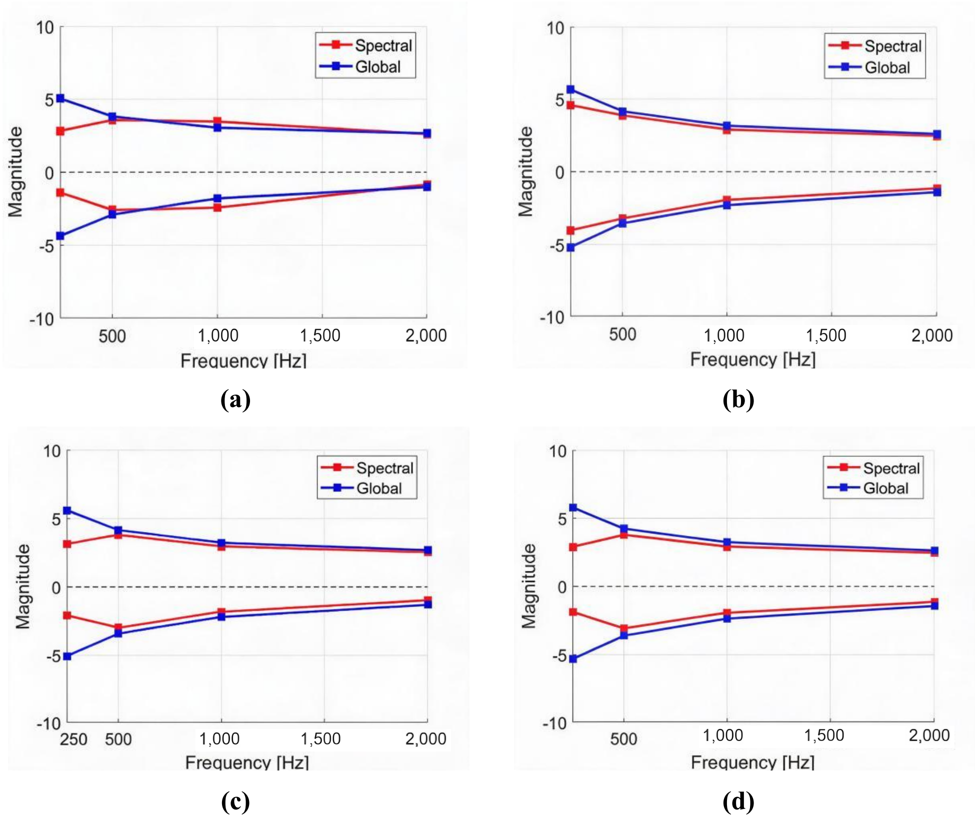

Figure 15. Real (upper) and imaginary (lower) components of the estimated complex ground impedance using the spectral-band method and the traditional global-band method based on 1/1-octave band: **(a)** Test 1; **(b)** Test 2; **(c)** Test 3; **(d)** Test 4.

As shown in **Figure 15a**, for recently mown grassland, the spectral-band method yields real and imaginary parts of the acoustic impedance that increase with frequency below 500 Hz, remain nearly constant over the mid-frequency range (approximately 500–1,000 Hz), and then decrease beyond 1,000 Hz. This pattern reflects a frequency-dependent trend of "rising–stable–falling" across the spectrum.

In contrast, **Figure 15b** illustrates that for dry lawn, both the real and imaginary parts of the impedance obtained using the spectral-band method decrease steadily with increasing frequency. This behavior closely resembles that observed with the global-band method, indicating that, under such ground conditions, both methods exhibit similar representations of the frequency-dependent impedance characteristics.

Figure 15c,d present the impedance trends for freshly harvested farmland and compacted farmland. In both cases, the spectral-band method produces the impedance components that increase with frequency below 500 Hz and then decrease thereafter, exhibiting a "rising–falling" pattern. This trend is consistent with the results obtained using the 1/3-octave band method, suggesting that the spectral-band method is effective in capturing the key frequency-dependent behavior of the ground impedance, especially in the low- to mid-frequency range.

The results indicate that the spectral-band method still enables more accurate estimation of the frequency-dependent real and imaginary parts of the impedance for each band. In contrast, when applying the full-band method, the variation across frequencies is smoother and more continuous, which aligns with the results obtained using the 1/3-octave band.

When applying the full-band method, the estimated flow resistivity remains fixed at 100 kPa · s · m^{-2} across all four tests, regardless of frequency, as shown in **Figure 16**. This uniform result is due to the coarse parameter step size inherent in the full-band approach, which limits its sensitivity to subtle changes in the acoustic response.

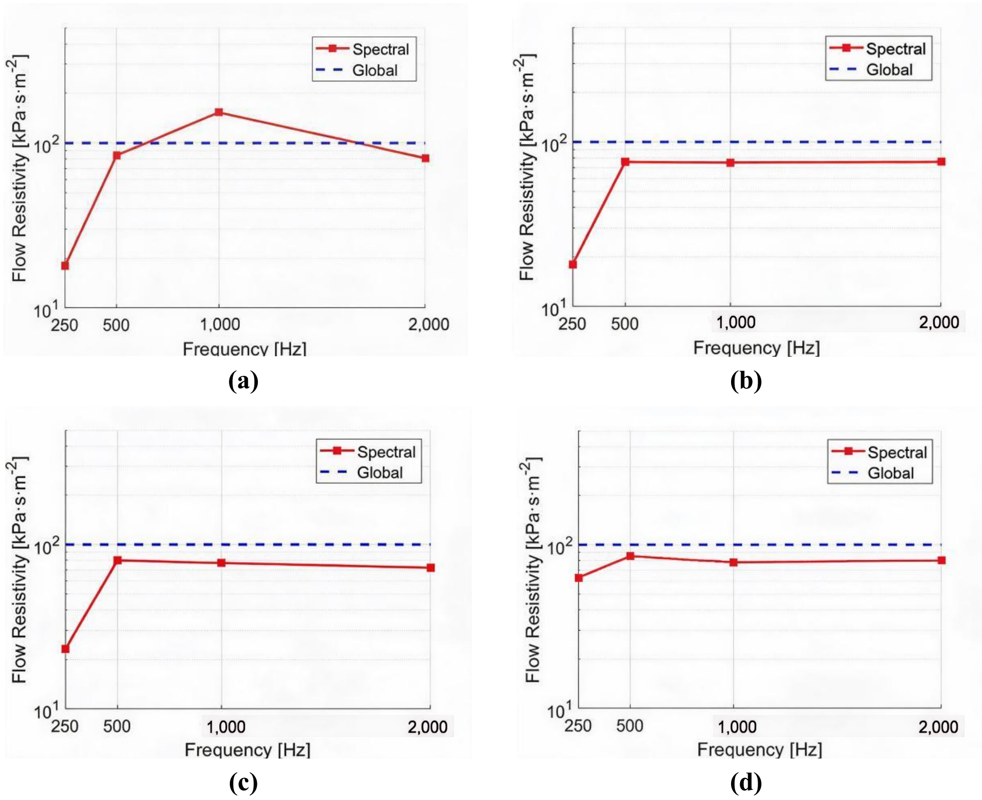

Figure 16. Relationship between the flow resistivities determined by the spectral-band method and by the traditional global-band method based on 1/1-octave band: **(a)** Test 1; **(b)** Test 2; **(c)** Test 3; **(d)** Test 4.

In contrast, the spectral-band method provides a more refined and adaptive estimation of the effective flow resistivity across different frequency bands, yielding values consistently lower than those of the full-band method in the 1/1-octave analysis. This improvement highlights the method's ability to resolve frequency-dependent characteristics more effectively. Notably, at 250 Hz, the estimated flow resistivity is significantly lower than at other frequencies. Rather than implying a directly measured reduction in sound propagation resistance, this result indicates a lower equivalent flow resistivity within the adopted impedance model. This low-frequency behavior is relevant to wind turbine sound propagation because low- and mid-frequency components can propagate over longer distances; however, the present validation remains limited to 250 Hz and above for the 1/1-octave case.

Moreover, a clear increasing trend in the flow resistivities is observed as frequency increases from 250 Hz to 500 Hz. Beyond 500 Hz, however, the values tend to plateau. These observations underscore the advantages of the spectral-band method in capturing more physically meaningful trends and enabling more accurate modeling of the ground impedance behavior across a wide frequency range.

4.2.3. Comparison between 1/3-octave and 1/1-octave bands

The above analysis verifies the applicability of the spectral-band method under the 1/1-octave band condition. The results suggest that the spectral-band method remains effective when implemented with 1/1-octave bands, providing an acceptable level of fitting accuracy for practical applications. Although the frequency resolution is lower than that of the 1/3-octave analysis, the overall agreement with the measured data is still satisfactory over the validated frequency range. An additional benefit of the 1/1-octave implementation is its computational efficiency. Because the number of frequency bands is reduced, fewer impedance parameters need to be estimated, which simplifies the fitting procedure and shortens the calculation time. The computational demand on both memory and central processing unit (CPU) resources is therefore lower. For applications such as real-time acoustic evaluation or the processing of large measurement datasets, these practical advantages may outweigh the modest reduction in frequency resolution.

However, it is important to note that the broader bandwidth of the 1/1-octave band leads to reduced frequency resolution, potentially masking fine acoustic features and making it difficult to capture narrowband variations. This limitation may affect the accuracy of applications requiring high spectral resolution, such as wind farm noise prediction and the characterization of frequency-dependent ground acoustic impedance in wind farm environments. Therefore, for studies that demand detailed frequency-dependent analysis, the 1/3-octave band, or even finer narrowband spectral analysis, remains the more appropriate choice. The present data do not address octave bands below 250 Hz; future work should extend the measurement geometry and validation range to lower frequencies that are also important for wind turbine low-frequency sound propagation.

4.3. Uncertainty analysis

The two-microphone method suffers from numerous sources of uncertainty, such as microphone positioning, source location, amplitude errors in microphone responses, and wind noise, all of which can significantly affect the transfer function. These errors in the transfer function can lead to considerable uncertainties in the determination of the surface impedance [43]. Therefore, the uncertainties in both the transfer function and the derived flow resistivity are presented and discussed.

The uncertainty analysis is performed on the Test 3 measurement configuration. On one hand, the uncertainties in the microphone height, source height, and their horizontal separation are considered. Following Kruse and Mellert [43], deviations of ±2 cm in height and ±5 cm in horizontal distance are imposed, respectively. On the other hand, the transfer function T is evaluated with an introduced deviation of 0.2 dB. The transfer function T is defined as the ratio of the sound pressure at the upper microphone to that at the lower microphone, and the corresponding results are shown in **Figure 17**. It is evident from the figure that the distance error exerts only a modest effect on the estimated ground impedance, well within the acceptable range, and its magnitude is notably smaller than that found in the work of Kruse and Mellert [43]. The effect of the transfer function error is almost negligible. This difference is likely due to the fact that the smaller geometrical dimensions in the work of Kruse and Mellert [43] make the results more sensitive to errors, whereas the larger dimensions employed in the present experiment substantially reduce such sensitivity.

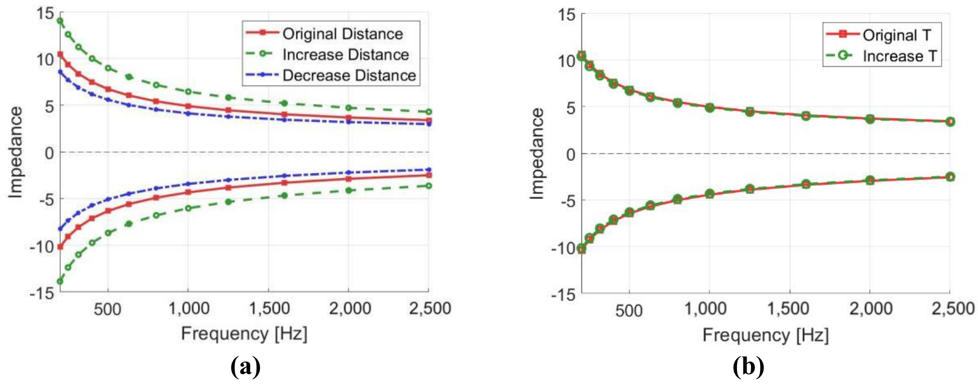

Figure 17. Effect of errors on the estimated ground impedance: **(a)** effect of distance error; **(b)** effect of transfer function error.

A total of four measurements were conducted in this study. Geometric positioning employed a tape measure with a resolution of 1 mm, and the deviations between measured and nominal values for the sound source height, microphone heights, and horizontal distance were all within ±10 mm. Given the relatively small spacing between measurement points, the influence of positioning deviations on the acoustic path difference and interference pattern is negligible. The maximum wind speed during measurement was 3.5 m/s, meeting the method's requirement of no greater than 5 m/s, and the effects of turbulence and temperature gradients were limited. The signal-to-noise ratio for each frequency band was no less than 15 dB, making the influence of background noise acceptable. Both the microphones and the loudspeaker were within their valid calibration periods, with a calibration accuracy of ±0.2 dB, ensuring that systematic errors are controllable. The maximum standard deviation across all frequency bands from the four independent measurements was 2.5 dB, which is below the judgment threshold of 4 dB, demonstrating good repeatability. In summary, all process-related errors in this measurement satisfy the validity criteria of the method, and the random errors are within an acceptable range.

5. Conclusion

In this study, a spectral-band method for determining the ground acoustic impedance in wind farm environments was proposed to improve the ground boundary condition used in wind turbine sound propagation modeling. The method is not intended to model wind turbine sound generation directly; rather, it provides frequency-dependent impedance inputs for propagation calculations over natural and agricultural ground surfaces. Based on four experimental test cases, the following conclusions were drawn:

1. Compared with the conventional global-band method, the spectral-band method significantly reduced the fitting error between the calculated and measured SPL differences across multiple tests.

2. The spectral-band method captured the more detailed frequency-dependent impedance variations. Although the resulting impedance curves are less smooth than those from the global-band method, they provide an improved local agreement with the measured SPL differences and therefore improve the reliability of parameter inversion.
3. The effective flow resistivity derived from the spectral-band method exhibits a non-monotonic spectral shape, generally rising toward the mid-frequency range and decreasing at higher frequencies. In contrast, the global-band method tends to overestimate the effective flow resistivity in both low- and high-frequency bands.
4. An empirical formula was established to estimate the spectral-band effective flow resistivities from the full-band flow resistivity. Validation results demonstrated that the proposed formula provides good overall consistency with the original spectral-band data, although isolated transition bands may still show noticeable discrepancies.
5. For ground acoustic impedance measurements relevant to wind farm sound propagation, the 1/3-octave band is more suitable than the 1/1-octave band when detailed frequency-dependent information is required. Its higher frequency resolution allows for better identification of acoustic features and spectral variations, thereby improving the accuracy and reliability of the inversion results.

In summary, the spectral-band method improves the accuracy and stability of ground acoustic impedance parameter inversion and provides an effective technical approach for specifying ground boundary conditions in wind turbine sound propagation models. The present validation is limited to flat natural or agricultural ground surfaces and to the frequency range covered by the measurement configuration. In particular, additional low-frequency validation below 200 Hz or below the 250-Hz octave band is required for a more complete assessment of wind turbine low-frequency sound propagation. Furthermore, current acoustic impedance models do not fully account for the complex mechanisms of sound-wave propagation and reflection at large incident angles, which may introduce systematic errors in the inversion results. Future work should focus on model corrections under large-angle incidence and extend the approach to more complex acoustic scenarios, such as irregular terrain, multi-layered ground structures, and vegetated wetlands.

Author contributions: Conceptualization, CM and WS; methodology, WY, WS; software, WY; validation, CM, WY and SS; formal analysis, SS and CX; investigation, CM and WY; resources, CM and WS; data curation, WY; writing—original draft preparation, WY and CM; writing—review and editing, WS and CX; supervision, WS; project administration, WS; funding acquisition, CM and WS. All authors have read and agreed to the published version of the manuscript.

Funding: This work was supported by the National Natural Science Foundation of China (No. 12502336), the 2024 Jiangsu Provincial Carbon Peaking and Carbon Neutrality Science and Technology Innovation Special Project (No. BT2024003) under the Jiangsu Province Department of Science and Technology, China, and the Yangzhou

Innovation Capability Enhancement Fund (No. YZ2023247) under the Yangzhou Science and Technology Bureau, China. This work was also supported by the starting grant of Yangzhou University, China, for Professor Wenzhong Shen.

Institutional review board statement: Not applicable. This study did not involve human participants or animals.

Informed consent statement: Not applicable.

Data availability statement: The data used in this study are available from the corresponding author upon reasonable request.

Conflict of interest: The authors declare that they have no competing interests.

AI use statement: During the preparation of this manuscript, the authors used an LLM tool solely for language refinement. No AI tools were used for data analysis, interpretation, or generation of scientific content. All outputs were critically reviewed and edited by the authors. The authors take full responsibility for the integrity and accuracy of the work.

References

1. Swadi M, Kadhim DJ, Salem M, et al. Investigating and predicting the role of photovoltaic, wind, and hydrogen energies in sustainable global energy evolution. Global Energy Interconnection. 2024; 7(4): 429–445.
2. Sun Z, Zhu W, Jané E, et al. Sound propagation analysis of a 10 MW wind turbine: Influence of the tower, operational states, and atmospheric conditions. Renewable Energy. 2025; 255: 123842.
3. Attenborough K. Review of ground effects on outdoor sound propagation from continuous broadband sources. Applied Acoustics. 1988; 24(4): 289–319.
4. Kayser B, Gauvreau B, Ecotière D. Sensitivity analysis of a parabolic equation model to ground impedance and surface roughness for wind turbine noise. The Journal of the Acoustical Society of America. 2019; 146(5): 3222–3231.
5. Kruse R. Application of the two-microphone method for in-situ ground impedance measurements. Acta Acustica United with Acustica. 2007; 93(5): 837–842.
6. ANSI S1.18-1999. Template Method for Ground Impedance. 1999.
7. Salomons EM. Computational Atmospheric Acoustics. Springer Science & Business Media; 2001.
8. Delany ME, Bazley E. Acoustical properties of fibrous absorbent materials. Applied Acoustics. 1970; 3(2): 105–116.
9. Martens M, van der Heijden L, Walthaus H, et al. Classification of soils based on acoustic impedance, air flow resistivity, and other physical soil parameters. The Journal of the Acoustical Society of America. 1985; 78: 970–980.
10. Bérengier M, Stinson M, Daigle G, et al. Porous road pavements: Acoustical characterization and propagation effects. The Journal of the Acoustical Society of America. 1997; 101: 155–162.
11. NORDTEST. Nordtest Method (NT ACOU 104)—Ground Surfaces: Determination of the Acoustic Impedance. NORDTEST; 1999.
12. Nyborg CM, Shen WZ. New measurement technique for ground acoustic impedance in wind farm. Renewable Energy. 2021; 164: 791–803.
13. Guillaume G, Faure O, Gauvreau B, et al. Estimation of impedance model input parameters from in situ measurements: Principles and applications. Applied Acoustics. 2015; 95: 27–36.
14. Liu C, Georgiou F, Hornikx M. Characterisation of the acoustic impedance of vegetated roofs with a multiple-geometry approach. Applied Acoustics. 2022; 199: 108997.
15. Cobb FA, Vecchiotti A, Turo D, et al. Experimental investigation of the variance of ground impedance measurments in coastal environments. The Journal of the Acoustical Society of America. 2022; 151: A117.
16. Ray EF. Applications of attenuations and reflections in ISO 9613-2, Acoustics-Attenuation of sound during

propagation outdoors-Part 2: General method of calculation. In: INTER-NOISE and NOISE-CON Congress and Conference Proceedings, NoiseCon04, Baltimore, MD, Proceedings of the National Conference on Noise Control Engineering; 12–14 June 2004; Baltimore, MD, USA. Institute of Noise Control Engineering; 2004. pp. 834–842.

17. IEC 61400-11. Wind Turbines—Part 11: Acoustic Noise Measurement Techniques. 2012.
18. Miki Y. Acoustical properties of porous materials-Modifications of Delany–Bazley models. Journal of the Acoustical Society of Japan (E). 1990; 11: 19–24.
19. Dragna D, Attenborough K, Blanc-Benon P. On the inadvisability of using single parameter impedance models for representing the acoustical properties of ground surfaces. The Journal of the Acoustical Society of America. 2015; 138(4): 2399–2413.
20. Attenborough K. Ground parameter information for propagation modeling. The Journal of the Acoustical Society of America. 1992; 92: 418–427.
21. Attenborough K. Acoustical impedance models for outdoor ground surfaces. Journal of Sound and Vibration. 1985; 99(4): 521–544.
22. Attenborough K, Bashir I, Taherzadeh S. Outdoor ground impedance models. The Journal of the Acoustical Society of America. 2011; 129(5): 2806–2819.
23. Attenborough K. Sound propagation close to the ground. Annual Review of Fluid Mechanics. 2002; 34: 51–82.
24. Raspet R, Sabatier JM. The surface impedance of grounds with exponential porosity profiles. The Journal of the Acoustical Society of America. 1996; 99: 147–152.
25. Attenborough K. Acoustical characteristics of porous materials. Physics Reports. 1982; 82: 179–227.
26. Attenborough K. Acoustical characteristics of rigid fibrous absorbents and granular materials. The Journal of the Acoustical Society of America. 1983; 73: 785–799.
27. Attenborough K. On the acoustic slow wave in air-filled granular media. The Journal of the Acoustical Society of America. 1987; 81: 93–102.
28. Wu J, Wang J, Sun Z, et al. Determination of the Parameters of Ground Acoustic-Impedance in Wind Farms. Sustainability. 2022; 14(23): 15489.
29. Fuchs A, Haider M. Improvements in Measuring Acoustic Impedance of Outdoor Ground Surfaces. In: Proceedings of Forum Acusticum Euronoise 2025: 11th Convention of the European Acoustics Association; 23–26 June 2025; Málaga, Spain.
30. Ghiasvand A, Javaherian A, Amirmazlaghani M, et al. Determining acoustic impedance cube by inverting seismic data using feedforward and radial basis neural networks in an Iranian oilfield. Scientific Reports. 2026; 16: 4221.
31. Schmid JD, Bauerschmidt P, Gurbuz C, et al. Physics-informed neural networks for acoustic boundary admittance estimation. Mechanical Systems and Signal Processing. 2024; 215: 111405.
32. Xia Y, Borrel-Jensen N, Engsig-Karup AP, et al. Neural impedance boundary (NeIB): A neural-network based framework for acoustic surface impedance estimation utilizing sparse measurement data. In: INTER-NOISE and NOISE-CON Congress and Conference Proceedings, INTER-NOISE24, Nantes, France, Pages 6993–7998, Proceedings of the 53rd International Congress & Exposition on Noise Control Engineering; 25–29 August 2024, Nantes, France. Institute of Noise Control Engineering; 2024. pp. 7392–7402.
33. Vecchiotti A, Ryan TJ, Vignola JF, et al. Atmospheric sound propagation over rough sea: Numerical evaluation of equivalent acoustic impedance of varying sea states. Acoustics. 2024; 6(2): 489–508.
34. Attenborough K. An Approximate Analytical Method for Predicting Attenuation Due to Ground Effect. Acoustics. 2026; 8(2): 30.
35. Vecchiotti A, Ryan TJ, Cobb FA, et al. Investigation of engineering models for sound propagation in a near-shore environment. Applied Acoustics. 2022; 199: 108991.
36. Cao JF, Nyborg CM, Feng J, et al. A new multi-fidelity flow-acoustics simulation framework for wind farm application. Renewable and Sustainable Energy Reviews. 2022; 156: 111939.
37. Colas J, Emmanuelli A, Dragna D, et al. Wind turbine sound propagation: Comparison of a linearized Euler equations model with parabolic equation methods. The Journal of the Acoustical Society of America. 2023; 154: 1413–1426.
38. Nyborg CM, Bolin K, Karasalo I, et al. An inter-model comparison of parabolic equation methods for sound propagation from wind turbines. The Journal of the Acoustical Society of America. 2023; 154: 1299–1314.
39. Naylor J, Qin Q. Laboratory Validation of 3D Model and Investigating Its Application to Wind Turbine Noise Propagation over Rough Ground. Wind. 2024; 4(4): 363–375.
40. Horsman SG, Shu Y, King EA. Offshore wind turbine noise propagation and the. In: INTER-NOISE and

NOISE-CON Congress and Conference Proceedings, INTER-NOISE24, Nantes, France, Pages 3993–4995, Proceedings of the 53rd International Congress & Exposition on Noise Control Engineering; 25–29 August 2024, Nantes, France. Institute of Noise Control Engineering; 2024. pp. 4916–4917.

41. Nguyen PD, Hansen KL, Zajamsek B, et al. Multi-input model uncertainty analysis for long-range wind farm noise predictions. Applied Acoustics. 2023; 205: 109276.
42. Fauri G. Measurement of the Ground Impedance in Wind Farms [Master's thesis]. Technical University of Denmark (DTU); 2019.
43. Kruse R, Mellert V. Effect and minimization of errors in in situ ground impedance measurements. Applied Acoustics. 2008; 69: 884–890.